Eremoxylarins D–J, Antibacterial Eremophilane Sesquiterpenes Discovered from an Endolichenic Strain of Xylaria hypoxylon

Alice Miral, Solenn Ferron, Isabelle Rouaud, Dinmukhammed Slyambayev, Latifa Bousarghin, Charline Camuzet, Sandrine Belouzard, Karin Séron, Pierre Le Pogam, Sylvain Tranchimand, et al.

Eremoxylarins D–J, Antibacterial Eremophilane Sesquiterpenes Discovered from an Endolichenic Strain of *Xylaria hypoxylon*.

Alice Miral,[†] Solenn Ferron,[†] Isabelle Rouaud,[†] Dinmukhammed Slyambayev,[†] Latifa Bousarghin,[‡] Charline Camuzet,[§] Sandrine Belouzard,[§] Karin Séron,[§] Pierre Le Pogam,[^] Sylvain Tranchimand,[○] and Sophie Tomasi[†*]

[†] *Univ Rennes, CNRS, ISCR (Institut des Sciences Chimiques de Rennes)-UMR 6226, Rennes, France.*

[‡] *INSERM, Univ. Rennes, INRAE, CHU Rennes, Nutrition Metabolisms and Cancer (NuMeCan), UMR-1317, Biosit, MRic/ISFR, Rennes, France*

[§] *Univ. Lille, CNRS, Inserm, CHU Lille, Institut Pasteur de Lille, U1019 – UMR9017 – Center for Infection and Immunity of Lille (CIIL), F-59000 Lille, France.*

[^] *Équipe Chimie des substances naturelles" BioCIS, CNRS, Université Paris-Saclay, 17, avenue des Sciences, 91400, Orsay, France.*

[○] *ENSCR, CNRS, ISCR (Institut des Sciences Chimiques de Rennes)-UMR 6226, Rennes, France.*

An endolichenic strain of the Ascomycetaceous *Xylaria hypoxylon*, cultivated alone or in co-culture with another endolichenic fungus *Dendrothyrium variisporum*, produced seven new bioactive eremophilane sesquiterpenes eremoxylarins D-J (**1**–**7**). The isolated compounds disclosed a high similarity with the eremophilane core of the bioactive integric acid, and structures were elucidated by 1D and 2D NMR spectra and ECD analyses. Eremoxylarins D, F, G and I showed a selective activity against Gram-positive bacteria such as methicillin-resistant *Staphylococcus aureus* with MIC values between 0.39 and 25 µg/mL. Eremoxylarin I, the most antibacterial active sesquiterpene, was also active against HCoV-229E at a concentration non-toxic to hepatoma Huh-7 cell line with an IC_{50} of 18.1 µM and a CC_{50} of 46.6 µM.

Nature provides the most tremendous reservoir of microorganisms able to produce potentially bioactive compounds.[1–3] As an example, lichens, which represent symbiotic relationships between a mycobiont with one or more photobiont partners (*e. g.* algae and/or cyanobacteria), include a diverse array of associated microscopic organisms and are therefore considered as an example of an holobiont.[4] Moreover, it is suggested that lichens and their microbiota interact through the production of antimicrobial agents potentially regulating microorganism-microorganism and microorganism-host interactions.[5,6] Among this microflora, research on lichen-associated fungi and their secondary metabolism is getting increasing attention over the last decades and these organisms have proven to be prolific sources of novel metabolites that are of significant biological interest.[7,8] In a previous study, we obtained 68 fungal isolates distributed in 43 phylogenetic groups from the crustaceous lichen *Rhizocarpon geographicum* collected in Finistère, France.[9] During the isolation process, one species, *Xylaria hypoxylon*, exhibited interesting antagonistic interactions with other fungi such as *Dendrothyrium variisporum*. *X. hypoxylon* is known to occupy different ecological niches with a wide host range and a widespread global occurrence.[10–13] It encounters a vast diversity of competitors, likely inducing the expression of a broad set of genes to successfully defend its habitat and communicate with such a large diversity of organisms.[14] Indeed, previous studies on *X. hypoxylon*[15,16] revealed that this fungus was able to produce antimicrobial compounds against Gram-positive bacteria. A screening performed against *Staphyloccoccus aureus* revealed the significant activity of a crude extract obtained from a 14 days *X. hypoxylon* culture, fueling our interest in undertaking a mycochemical investigation on this species. A bioactivity-guided fractionation workflow, based on *in vitro* antibacterial activity assays against human pathogenic bacteria, led to the isolation and structural elucidation of seven novel bioactive eremophilane sesquiterpenes eremoxylarins D–J (**1**-**7**), analogous to other compounds produced by *Xylariaceous* fungi such as integric acid, compound 07H239-A[17] or eremoxylarins A to C[18].

These compounds have already shown various biological activities: anti-HIV[19] and antiplasmodial[20] (integric acid), cytotoxicity toward cancer cell lines[17,18] (07H239-A and eremoxylarin C) or antibacterial activity against *S. aureus* and *Pseudomonas aeruginosa*[21] (eremoxylarins A and B). To confirm the interest of this eremophilane core, their antibacterial activities against different bacteria were evaluated as well as their antiviral activity against a human coronavirus (HCoV-229E). This virus is responsible for the common cold in humans and can serve as a model for highly pathogenic coronaviruses such as severe acute respiratory coronavirus 2 (SARS-CoV-2) causing COVID-19, or Middle-East respiratory syndrome coronavirus (MERS-CoV).

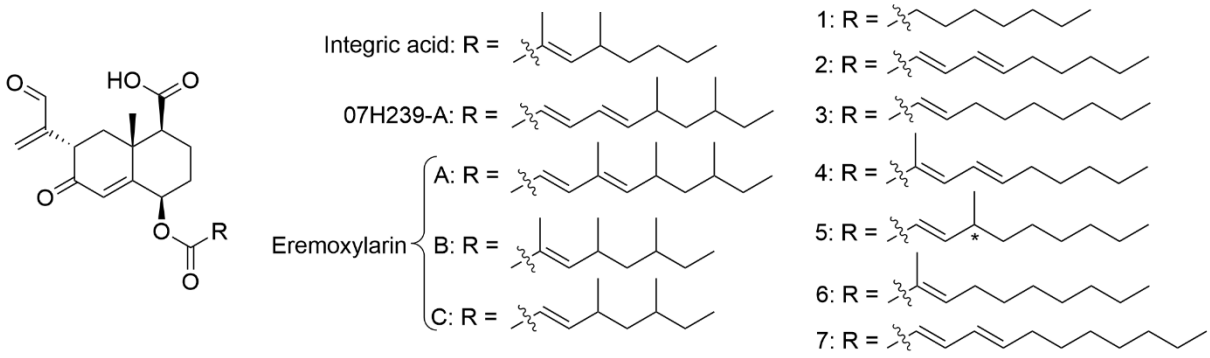

Results and discussion

Compound isolation, prioritization, and SMART-based dereplication. Compounds **1**–**7** were isolated from a solid co-culture (350 Petri dishes) of *D. variisporum* and *X. hypoxylon.* The antibacterial activities of the fractions and their HPLC-DAD-ESI-MS profiles guided us to further consider fractions F6, F7 and F8 (F6-F8) that were pooled (229.15 mg). The HSQC data retrieved from this fraction were garnered in a .txt file and subsequently uploaded into the SMART platform (Small Molecule Accurate Recognition Technology).[22] This artificial intelligence-based tool aims at generating structure candidates from HSQC data, based on a deep convolutional neural network architecture incorporating the HSQC information related to

more than 50,000 natural products. SMART analysis revealed integric acid to be the preferred hit.[19] This evidence was corroborated by electrospray (ESI) mass spectrometric analysis (see Figure S1) of all seven molecules showing a common fragment ion at *m/z* 261 (possibly corresponding to a $C_{15}H_{17}O_4$ formula), consistent with the core decalin unit of integric acid, obtained after cleavage of the ester group followed by dehydration,[19] and a fragment at *m/z* 215 (corresponding to a $C_{14}H_{15}O_2$ unit) consistent with the subsequent loss of a CH_2O_2 unit from this decalin platform. Further purification was carried out on F6-F8 by semi-preparative reversed phase HPLC to afford seven new eremophilane sesquiterpenes named eremoxylarins D–J (**1**–**7**), exclusively differing by the nature of the acyl side chain. Noteworthy, LC-MS analysis of a crude extract obtained after a mono-culture of the strain *X. hypoxylon* underlined its capacity to produce this series of sesquiterpenes in axenic conditions.

Structure Elucidation. Compound **1** was obtained as amorphous solid with the molecular formula, $C_{23}H_{32}O_6$ being deduced from HR-ESIMS measurements, suggesting 8 indices of hydrogen deficiency. The ^{1}H NMR data showed (Table 1) distinct signals for two methyls (a singlet at δ 1.51 and a broad triplet at δ 0.87), two methines (as doublet of doublet at 2.48 and 3.74), an oxygen-bearing methine (as a broad triplet at δ 5.46), an olefinic methine (a singlet at δ 5.95), a vinyl group (as two singlets at δ 6.44 and δ 6.31), and an aldehydic group (a singlet at δ 9.55). The remaining signals were assigned to 9 methylene groups, as confirmed by the 1D JMOD NMR spectrum which also displayed a quaternary sp^3 carbon (at δ 38.9) and three carbonyl carbons resonating above 170 (δ_C 172.5, 174.0, 197.0). The last carbonyl carbon at δ 193.9 was assigned through the HSQC spectrum to the aldehydic group. Obvious COSY and HMBC correlations and comparison with data reported for integric acid[19] confirmed the presence of the eremophilane decalin unit. In addition, HMBC cross-peaks for the methylene protons H-2′ at δ 2.37 and H-3′ at δ 1.67 with the carbonyl C-1″ group at δ 172.5 determined the bonding of the sesquiterpene unit to the side chain through an ester. Finally, the 2D TOCSY

spectrum confirmed the spin system corresponding to an aliphatic side chain containing six methylene groups. The relative configuration of compound **1** was established based on the magnitude of the vicinal coupling constants and of the NOESY spectrum (Table S1). First, the coupling constants of H-7 ($^3J_{H6ax}$ and $^3J_{H6eq}$ = 14.4 and 4.3 Hz, respectively), revealed its axial orientation. In addition, the NOESY correlation peaks between H-7 and H-14 (methyl group) and between H-14 and H-3 (δ 2.27) and H-6 (at δ 2.13) ascribed these protons to the same face of the chair conformation corresponding to the axial orientation for H-14 and H-3 and to the equatorial orientation for H-6. The equatorial assignment of H-1 was supported by its coupling constant of 4 Hz with the two H-2 protons. Finally, H-4 was placed in the axial orientation through its coupling constants and NOE data with H-2ax, H-3eq, H-6ax (Figures 1 and S2).

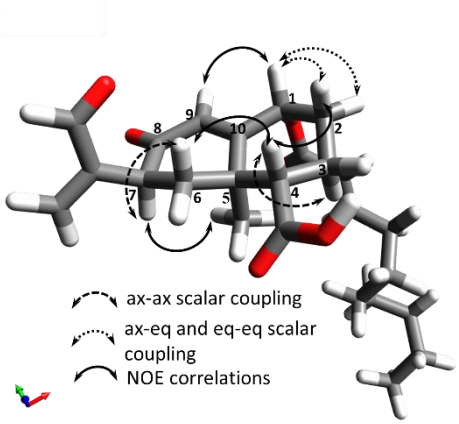

Figure 1. 3D structure of compound **3** realized with Avogadro 1.2 software (http://avogadro.cc/)

Table 1. ^{1}H (500 MHz) and ^{13}C (125 MHz) NMR spectral data of eremoxylarins D-J (**1**–**7**)

	eremoxylarin D (**1**)			eremoxylarin E (**2**)			eremoxylarin F (**3**)			eremoxylarin G (**4**)			eremoxylarin H (**5**)			eremoxylarin I (**6**)			eremoxylarin D (**7**)		
Position	δ_c	δ_H	*J* in Hz	δ_c	δ_H	*J* in Hz	δ_c	δ_H	*J* in Hz	δ_c	δ_H	*J* in Hz	δ_c	δ_H	*J* in Hz	δ_c	δ_H	*J* in Hz	δ_c	δ_H	*J* in Hz
1	73.7, CH	5.46	bt (4.0)	73.7, CH	5.51	bt (3.0)	73.8, CH	5.49	bt (3.0)	74.1, CH	5.52	bt (3.0)	73.6, CH	5.50	bt (3.0)	74.0, CH	5.51	bt (3.0)	73.7, CH	5.5	bt (2.6)
2eq	30.4, CH_2	2.08	m	30.5, CH_2	2.12	m	30.5, CH_2	2.10	m	30.5, CH_2	2.13	m	30.5, CH_2	2.10	m	30.6, CH_2	2.09	m	30.5, CH_2	2.10	m
2ax		1.83	m		1.89	dt (14.2, 3.9)		1.88	dt (14.1, 3.5)		1.89	m		1.87	m		1.86	m		1.88	dt (14.1, 3.7)
3ax	21.0, CH_2	2.27	m	21.0, CH_2	2.30	m	21.2, CH_2	2.30	m	21.2, CH_2	2.29	m	21.0, CH_2	2.29	m	21.2, CH_2	2.29	m	21.1, CH_2	2.31	m
3eq		1.83	m		1.83	m		1.82	m		1.83	m		1.83	m		1.81	m		1.83	m
4	53.8, CH	2.48	dd (13.3, 3.1)	53.9, CH	2.50	dt (12.9, 3.2)	54.1, CH	2.49	dd (12.4, 3.1)	53.9, CH	2.50	dt (13.1, 3.4)	53.8, CH		dd (13.4, 4.3)	54.0, CH	2.49	dd (12.9, 2.8)	53.9, CH	2.5	dd (12.9, 2.8)
5	38.9, Cq			39.0, Cq			38.9, Cq			38.9, Cq			39.0, Cq			38.9, Cq			38.9, Cq		
6ax	43.9, CH_2	2.37	m	44.0, CH_2	2.40	m	44.1, CH_2	2.39	tapp (13.9)	44.0, CH_2	2.40	m	44.0, CH_2	2.40	m	44.0, CH_2	2.40	tapp (13.9)	43.9, CH_2	2.40	tapp (13.9)
6eq		2.13	dd (13.3, 4.3)		2.12	m		2.13	dd (13.3, 4.3)		2.13	m		2.14	m		2.15	dd (13.4, 4.4)		2.13	m
7	44.4, CH	3.74	dd (14.4, 4.3)	44.5, CH	3.75	dd (14.4, 4.3)	44.7, CH	3.74	dd (14.5, 4.3)	44.5, CH	3.75	dt (14.5, 4.7)	44.4, CH	3.75	dd (14.5, 4.3)	44.5, CH	3.75		44.5, CH	3.75	dd (14.5, 4.3)
8	197.0, Cq			197.0, Cq			197.1, Cq			197.1, Cq			197.0, Cq			197.2, Cq		dd (14.4, 4.2)	197.0, Cq		
9	129.9, CH	5.95	s	130.0, CH	5.99	s	130.1, CH	5.98	s	130.0, CH	5.99	s	129.9, CH	5.98	s	130.0, CH	5.98	s	130.0, CH	5.98	s
10	160.4, Cq			160.3, Cq			160.3, Cq			160.4, Cq			160.2, Cq			160.6, Cq			160.3, Cq		
11	149.7, Cq			149.7, Cq			149.6, Cq			149.7, Cq			149.6, Cq			149.7, Cq			149.7, Cq		
12a	136.7, CH_2	6.44	s	136.7, CH_2	6.44	s	136.8, CH_2	6.44	s	136.7, CH_2	6.44	s	136.7, CH_2	6.44	s	136.8, CH_2	6.44	s	136.7, CH_2	6.44	s
12b		6.31	s		6.31	s		6.31	s		6.31	s		6.31	s		6.31	s		6.31	s
13	193.9, CH	9.55	s	194.0, CH	9.55	s	193.9, CH	9.55	s	193.9, CH	9.55	s	193.7, CH	9.55	s	193.9, CH	9.55	s	193.8, CH	9.55	s
14	20.0, CH_3	1.51	s	20.0, CH_3	1.51	s	20.0, CH_3	1.50	s	20.0, CH_3	1.53	s	19.8, CH_3	1.51	s	20.0, CH_3	1.52		20.0, CH_3	1.51	s
15	174.0, Cq			174.0, Cq			174.0, Cq			174.1, Cq			173.9, Cq			174.2, Cq		s	174.0, Cq		
1'	172.5, Cq			166.0, Cq			165.4, Cq			167.3, Cq			165.5, Cq			166.9, Cq			166.0, Cq		
2'	35.0, CH_2	2.37	m	119.3, CH	5.89	d (15.4)	122.1, CH	5.88	dt (15.6, 1.5)	125.7, Cq			120.3, CH	5.85	d (15.4)	128.5, Cq			119.9, CH	5.89	d (15.4)
3'	25.6, CH_2	1.62	m	146.5, CH	7.29	dd (15.4, 10.0)	151.1, CH	6.99	dt (15.6, 7.1)	140.0, CH	7.20	d (11.3)	155.9, CH	6.89	dd (15.7, 8.0)	143.8, CH	6.82	tq (7.5, 1.3)	146.4, CH	7.29	dd (15.3, 10.0)
4'	29.7, CH_2	1.62 (4'a)	m	129.3, CH	6.31	m	32.9, CH_2	2.25	m	126.8, CH	6.48	m	37.2, CH	2.36	m	29.2, CH_2	2.23	m	129.3, CH	6.33	m
		1.30 (4'b)	m																		
5'	29.7, CH_2	1.62 (5'a)	m	146.0, CH	6.29	m	28.8, CH_2	1.48	m	144.7, CH	6.20	dt (14.6, 7,6)	36.7, CH_2	1.37	m	29.8, CH_2	1.32	m	146.0, CH	6.29	m
		1.30 (5'b)	m																		
6'	32.4, CH_2	1.30	m	33.6, CH_2	2.19	m	29.7, CH_2	1.32	m	33.8, CH_2	2.22	m	27.9, CH_2	1.30	m	29.3, CH_2	2.23	m	33.6, CH_2	2.21	m
7'	23.3, CH_2	1.30	m	29.1, CH_2	1.45	m	29.8, CH_2	1.32	m	29.3, CH_2	1.45	m	29.8, CH_2	1.30	m	29.8, CH_2	1.32	m	29.7, CH_2	1.30	m
8'	14.3, CH_3	0.87	m	32.1, CH_2	1.31	m	32.5, CH_2	1.32	m	32.1, CH_2	1.33	m	32.5, CH_2	1.30	m	32.5, CH_2	1.29	m	29.4, CH_2	1.45	m
9'				23.1, CH_2	1.31	m	23.3, CH_2	1.32	m	23.1, CH_2	1.33	m	23.3, CH_2	1.30	m	23.3, CH_2	1.29	m	29.6, CH_2	1.30	m
10'				14.3, CH_3	0.88	m	14.3, CH_3	0.87	t (7.0)	14.3, CH_2	0.89	m	14.3, CH_3	0.87	m	14.3, CH_3	0.88	t (7.0)	32.5, CH_2	1.30	m
11'										12.8, CH_3	1.94	s	19.5, CH_3	1.05	d (6.7)	12.6, CH_3	1.84	s	23.3, CH_2	1.30	m
12'																			14.3, CH_3	0.87	t (7.0)

[a]Data were recorded at 500 MHz for proton and at 125 MHz for carbon in acetone-d_6.
(Supporting Information Figures S2-S53)
tapp: apparent triplet
nd: not determined

Analysis of the NMR spectra related to compounds **2**–**7** highlighted their structural similarity with compound **1**. All of them include an eremophilane core with identical substituents and the same relative configuration as **1**, as supported by the magnitude of the coupling constant values (Table 1) and key NOE correlations (Tables S2-S7, Supporting Information), and differed only in some modifications of the acyl side chains.

Compound **2,** with a molecular formula of $C_{25}H_{32}O_6$ supported by HR-ESIMS displayed a longer acyl chain with two additional carbons, and four olefinic carbons detected at δ 119.3, 129.3, 146.0, and 146.5, compared to **1**. The configuration of the 2′–3′ double bond was assigned as *E* through the measurement of the coupling constant of the doublet corresponding to the H-2′ proton ($^3J_{H2'\text{-}H3'}$ = 15.4 Hz). The configuration of the 4′–5′ double bond was, on the other hand, more complicated to determine as H-4' and H-5' formed an ABX system, and have signals almost superimposed with very complex multiplets. Fortunately, the acquisition of the COSY NMR spectrum in benzene-d_6 achieved separation of these overlapping signals and consequently the measurement of the coupling constant between H-4' and H-5' ($^3J_{H\text{-}4'\text{-}H\text{-}5'}$ =15 Hz (see Figure S14), led to the *E* configuration assignment to this double bond.

The molecular formula of **3** was determined to be $C_{25}H_{34}O_6$ from its HRESIMS data, and differed only from **2** by two additional hydrogen atoms. This loss of unsaturation was revealed by JMOD NMR spectrum to occur at the C-4′ and C-5′ s (see Figure S20 and Table 1). The remaining ethylenic bond retained the *E* configuration ($^3J_{H\text{-}2'\text{-}H\text{-}3'}$= 15.6 Hz).

The NMR data and elemental composition deduced from HRESIMS data ($C_{26}H_{34}O_6$) for compound **4** displayed an additional methyl group (C-11′) at δ 12.8 located on carbon 2′. The HMBC correlations between H-11′ and C-1′, C-2′ and C-3' and between H-3′ and C-11′, combined with the NOE cross signals between H-3′ and H-5' and the downfield shift of C-2′ (125.7) led to the location of this methyl group at C-2′. Interestingly, the NOE correlation between H-3′ and H-14 confirmed the axial orientation of H-14 and of the acyl chain. Careful

analysis of coupling constants ($^3J_{H\text{-}4'\text{-}H\text{-}5'=}$ 14.6 Hz; $^3J_{H3'\text{-}H4'}$ = 11.3 Hz) were both elucidated as *E* configuration of both olefinic bonds. It should be noted that compound **4** was isolated as a mixture with compound **3** in a 2:3-1:3 ratio.

Compounds **5** and **6**, both having the same molecular formula of $C_{26}H_{36}O_6$ [*m/z* 443.2439 ($[M-H]^-$) and 443.2438 ($[M-H]^-$), respectively] differed from compound **4** by a loss of two hydrogens, emphasizing the presence of only one indices of hydrogen deficiency on the acyl chain. The methyl group (CH_3-11′) of compound **5** was assigned to the C-4′ position due to the ^{1}H NMR signal multipliticity (1H, *d*, $^3J_{H4'\text{-}H11'}$ = 6.7 Hz) whereas it is located at C-2′ in compound **6** as shown by its HMBC correlations with C-1′, C-2′ and C-3′. The *E* configuration of the C-2′-C-3′ olefinic bond was established by the large coupling constant ($^3J_{H\text{-}2'\text{-}H\text{-}3'}$ = 15.4 Hz) for compound **5** and by the signal shape of the H-3′ as a triplet quadruplet ($^3J_{H3'\text{-}H4'}$ = 7.5 and $^4J_{H3'\text{-}H11'}$ = 1.3 Hz) for **6**. As for the other integric acid analogues[17-19] containing a methyl group located on an asymmetric carbon of the acyl side chain, the stereochemistry at C-4′ for compound **5** could not be determined.

Compound **7**, showed similar NMR data to compound **2**, except for the additional presence of two methylene groups also revealed by its $C_{27}H_{36}O_6$ molecular formula. The determination of the configuration of the two unsaturations followed the same process as described above and their configurations was elucidated as *E*.

The absolute configuration of compounds **1** to **7** was determined by comparison of experimental and TDDFT-calculated ECD spectra for the 1*R*, 4*S*, 5*R*, 7*S* enantiomer. The similarity of the theoretical spectra with the experimental spectra validated the absolute configuration for these compounds **1**–**7** as 1*R*, 4*S*, 5*R*, 7*S* (Figure 2), being identical to that of all integric acid analogues described so far.[19]

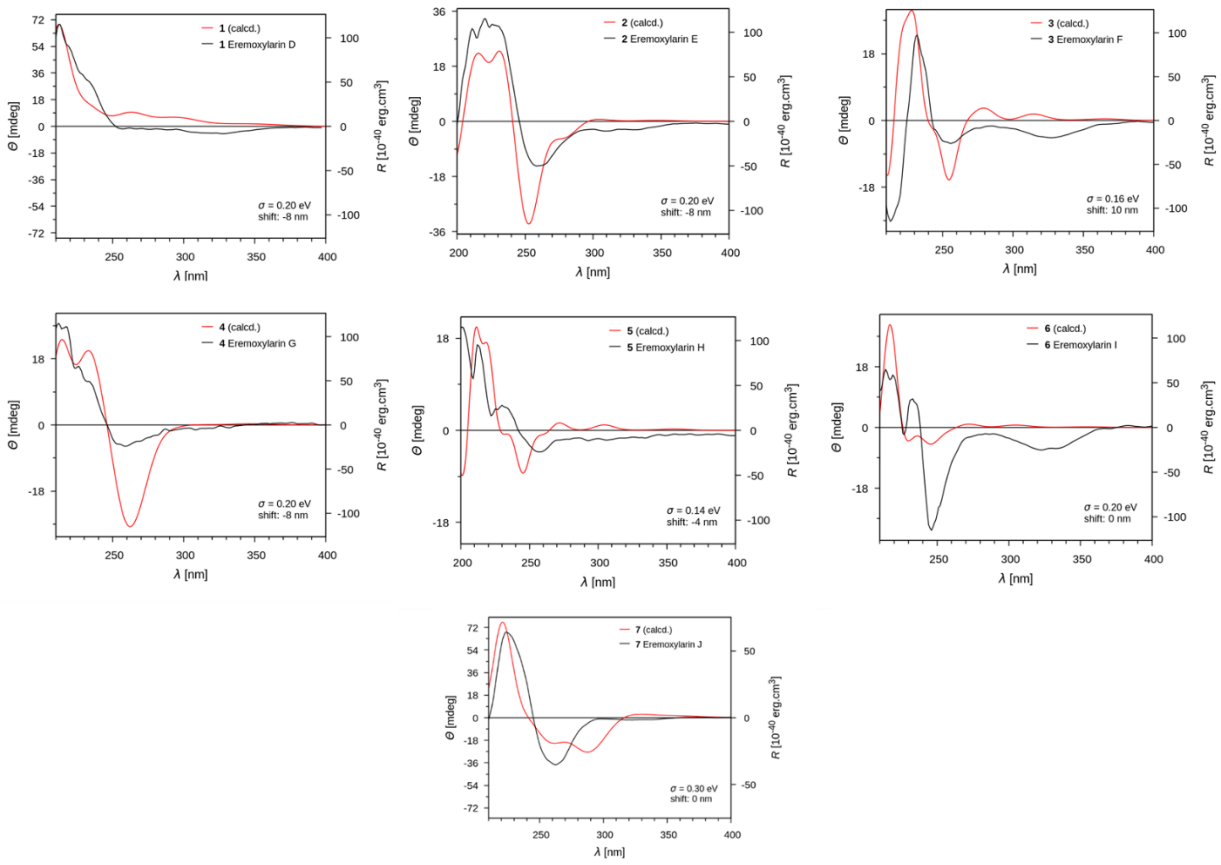

Figure 2. Superposition of experimental and calculated ECD spectra for the 1*R*, 4*S*, 5*R*, 7*S* configuration of compounds **1**–**7**

Antibacterial activity. The inhibitory activities of the isolated compounds were tested against a panel of pathogenic human bacterial strains (Table 2). The very low amounts of the new eremoxylarins E (**2**), H (**5**) and J (**7**) prevented us to evaluate their activity. Eremoxylarins D (**1**), F (**3**), G (**4**) and I (**6**) exhibited activity against Gram-positive bacteria [*Staphylococcus aureus*, methicillin-resistant *S. aureus* (MRSA) and *S. epidermidis*] with MIC values between 0.39 and 12.50 µg/mL. Eremoxylarin I (**6**) exerted the strongest (MIC values 0.78–3.10 µg/mL) and broadest activity against all tested Gram-positive pathogens. *Escherichia coli* and *Pseudomonas aeruginosa*, Gram-negative bacteria, were not susceptible to any of the compounds. Eremoxylarin D (**1**) with the shortest aliphatic chain was the least active

compound, highlighting the importance of chain length and/or rigidity in antibacterial activity as it was already described for other series[23].

Table 2. MIC evaluation of eremoxylarin D (**1**), eremoxylarin F (**3**), eremoxylarin G (**4**) and eremoxylarin I (**6**) against pathogenic human strains.

Strains	**MIC (µg/mL)**					
	1	**3**	**4**	**6**	**Gentamicin**	**DMSO**
Staphyloccocus aureus (CIP 53.156)	6.25	0.78	1.56	0.39	3.91	-
Methicillin-resistant S. aureus MRSA (DSM 13661)	12.50	1.56	3.10	1.56	250	-
S. epidermidis (CIP 53.124)	12.50	3.10	3.10	1.56	>250	
Escherichia coli (CIP 54.8)	-	-	-	-	3.91	-
Pseudomonas aeruginosa (CIP A22)	-	-	-	-	1.95	-

- : MIC > 50 µg/mL

Antiviral activity. Due to the activity of integric acid against HIV integrase,[19] compounds **1**, **3**, **4** and **6** were also evaluated for their activity against human coronavirus HCoV-229E. Experiments were performed with a recombinant HCoV-229E harboring a luciferase reporter gene to quantify infection, HCoV-229E-Luc. To mimic coronavirus entry in host cells, hepatoma cell line Huh-7 cells, expressing the cellular protease TMPRSS2, were infected. The TMPRSS2 protease is responsible for the cleavage of the spike protein which is necessary for the fusion of the viral envelope with the plasma membrane.[24] When it is not expressed, coronavirus enters via endocytosis and the fusion takes place in the endosomes. Each compound was added during infection. In parallel, the toxicity of the compounds on Huh-7 cells was determined by MTS assay and the CC_{50} were determined (Table 3). As shown in Figure 3,

it was not possible to determine the antiviral activity of compounds **1** and **3** because both are toxic at active concentrations. The compound **4** is less toxic but also less active and no major antiviral activity was observed up to 50 µM, the highest concentration tested in the antiviral assay. Finally, the only active compound at a concentration that does not affect cell viability was compound **6**, eremoxylarin I, with an IC_{50} of 18.1 µM and a CC_{50} of 48.1 µM. Even if eremoxylarin I is active at non-toxic concentration, the selectivity index of 2.57 is quite low. However, the fact that this compound is able to inhibit infection in both Huh-7 and Huh-7/TMPRSS2 cells is interesting because it means that it inhibits infection in the two pathways used by the virus to infect the cells.

Table 3. Toxicity of tested eremoxylarins on Huh-7 cells

Compound	CC_{50} (µM)
eremoxylarin D (**1**)	36.9 ± 22.4
eremoxylarin F (**3**)	37.7 ± 18.9
eremoxylarin G (**4**)	183.5 ± 62.8
eremoxylarin I (**6**)	48.1 ± 12.0

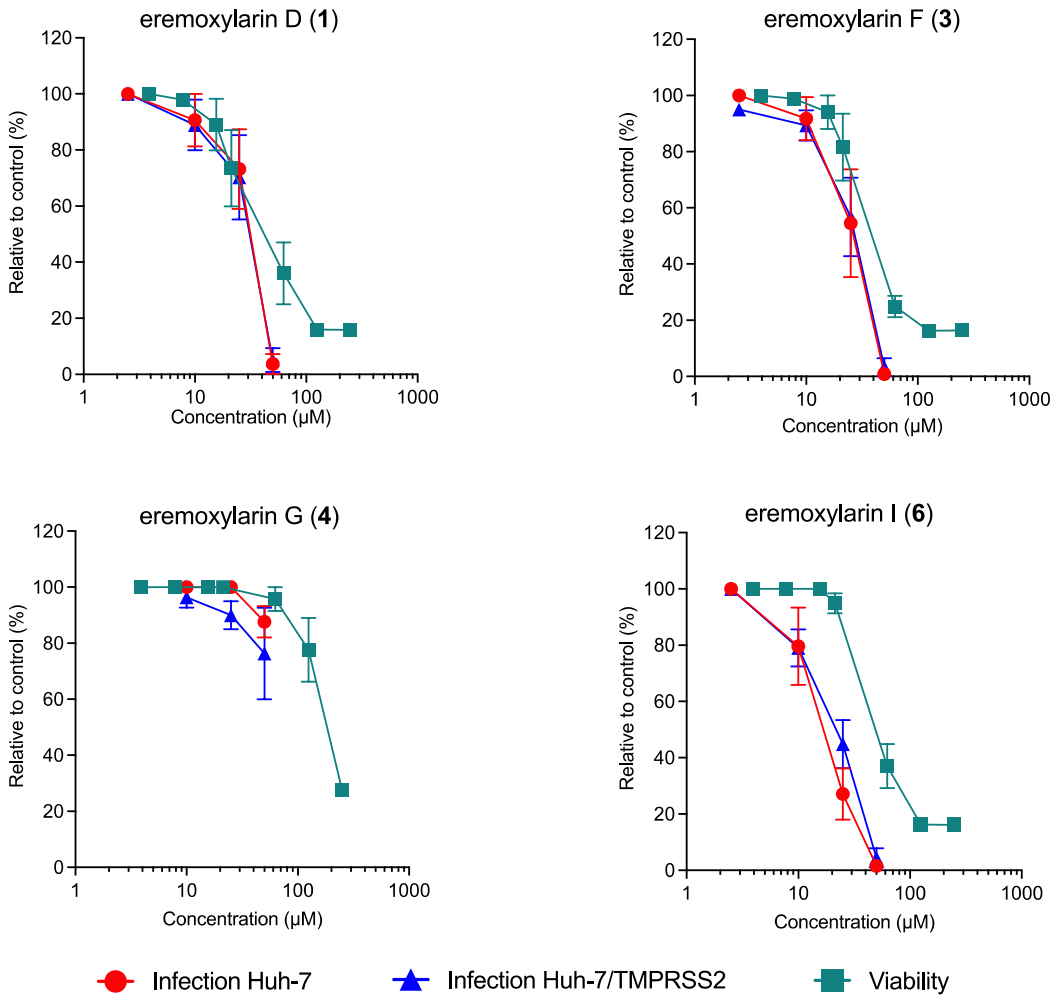

Figure 3. Antiviral and toxicity evaluation of eremoxylarin D (**1**), eremoxylarin F (**3**), eremoxylarin G (**4**) and eremoxylarin I (**6**). For each compound, toxicity and antiviral activity was determined with increasing concentrations. Huh-7 cells were incubated with each compound at the indicated concentrations for 24 h. MTS assay was performed to monitor cell viability. Results are expressed as mean ± SEM of 3 experiments. For antiviral assays, Huh-7 and Huh-7/TMPRSS2 cells seeded in 96-well plate were inoculated with HCoV-229E-Luc in the presence of compounds at indicated concentrations. Cells were lysed after 7 h post-inoculation and luciferase activity quantified. Data are expressed relative to the control DMSO. Results are expressed as mean ± SEM of 3 experiments.

It is interesting to note that, when compared to the other reported analogous structures (integric acid, compound 07H239-A or eremoxylarins A to C),[17,18] there are only small changes in the structure of the ester side chain: differences in length, double bonds and methyl groups at various positions. While subtle, these differences have a large impact on the biological activities of these compounds, meaning that the producing fungi are able to adapt themselves to various stimuli with only slight modifications on bioactive molecules with common cores.

Material and methods

General experimental procedures. All commercial reagents were purchased from Sigma Aldrich (Val de Reuil, France and St. Quentin Fallavier, France). An EasyPure (Barnstead™, ThermoFisher Waltham, MA, USA) water purification system was used to obtain HPLC and LC/MS grade water for chromatographic analysis. Deuterated solvents were purchased from Euriso-top (Gif-sur-Yvette, France). Extracts were analyzed using a Vanquish UHPLC coupled with a Thermo Q-Exactive (Thermo Fisher Scientific GmbH, Bremen, Germany) mass spectrometer (MS) and an ESI source operated with Xcalibur (version 2.2, ThermoFisher Scientific) software package. Data acquisition was realized under full scan switch (positive and negative) mode ionization from *m/z* 130 to 1200 at 70,000 resolution. The 1D (^{1}H and ^{13}C) and 2D (COSY, HSQC, HMBC and NOESY) NMR spectra were obtained on a Bruker 500 MHz spectrometer with a TCI cryo-probe (Bruker®, Billerica, MA, USA) at the PRISM core facility (Rennes, France). All spectra were acquired in acetone-d_6, and additional spectra were recorded in C_6D_6 for compounds **2** and **7**. Optical rotations were recorded using PerkinElmer 341 automatic polarimeter at 293 K at the sodium D line (589 nm); Electronic circular dichroism spectroscopy was performed in MeOH on a Jasco J-815 ECD spectrometer. The averages of triplicate scans were acquired and the CD signal of the MeOH was subtracted subsequently. The values of the ECD ellipticity (θ) were not corrected for the concentration and

are expressed in milli°. HRMS measurements for exact mass determination were performed on a Thermo Fisher Q-Exactive spectrometer for electrospray ionization at the CRMPO (Centre Régional de Mesures Physiques de l'Ouest), University of Rennes.

Fungal collection and taxonomy. The fungi *Dendrothyrium variisporum* (GenBank accession number OL891605) and *Xylaria hypoxylon* (GenBank accession number OL891603) were previously isolated from the lichen *Rhizocarpon geographicum* collected in Finistère, France.[9] *D. variisporum* and *X. hypoxylon* were individually maintained on yeast starch agar (YS; yeast extract 2 g, potato starch 10 g, agar 15 g in 1 L) as precultures for 14 days.

Large scale co-cultivation and isolation of compounds. Two 5 mm plugs from each pure culture, *D. variisporum* and *X. hypoxylon*, were cut and inoculated on opposite sides, pairwise to maximize confrontation zones, of the same 9 cm Petri dish containing about 25 mL of YS medium. In order to obtain enough crude extract for compound isolation, structural elucidation and bioassays, 350 YS medium filled plates were inoculated and then incubated at room temperature for 14 days. Co-cultures were crushed and extracted twice with CH_2Cl_2–EtOAc (v/v) (at a ratio of 5 plates: 250 mL of CH_2Cl_2–EtOAc) on an orbital rotary shaker at 120 rpm for 60 min followed by 60 min in a water-bath ultrasonicator. The mixture was filtered under reduced pressure through a Büchner funnel using a cheesecloth. CH_2Cl_2–EtOAc extract was collected, dried on anhydrous sodium sulfate and filtered through a coarse filter paper and the organic phase evaporated under reduced pressure to yield 3.5 g of dry organic extract. 1.5 g of CH_2Cl_2–EtOAc extract was then fractionated over a Chromabond Flash RS 25 SiOH column cartridges (Macherey-Nagel, Hoerdt, France). The mobile phase was composed of A (EtOAc), B (C_6H_{12}), C (MeOH) and D (H_2O). The following gradient was applied at a flow rate of 20 mL/min: from 0 to 5 min: 100% (B), from 5 to 6 min: 10% (A)–90% (B), from 6 to 10 min: 40% (A)–60% (B), from 10 to 16 min: 60% (A)–40% (B); from 16 to 24 min: 100% (A); from 24 to 32 min: 80% (A)–20% (C) ; from 32 min to 40 min: 50% (A)–50% (C); from 40 to

48 min: 20% (A)–80% (C) ; from 48 to 56 min: 100% (C) ; from 56 to 64 min: 80% (C)–20% (D) ; from 64 to 80 min: 50% (C)–50% (D) to afford 25 fractions (F1–F25). Their analytical HPLC profiles were analyzed with the following mobile phases A [0.1% formic acid in water] and B [0.1% formic acid in acetonitrile]. Fractions F6, F7 and F8 (F6–8), obtained with the gradient elution from 58%(B)-42%(A) to 38%(B)-62%(A), were combined (229.15 mg) and purified by HPLC on a semi-preparative RP column (Hypersil GOLD aQ (250 x 20, 5 µm) with H_2O + 0.1% FA:ACN + 0.1% FA mixture as mobile phase. The following gradient was applied at a flow rate of 8 mL/min: from 0 to 5 min: 100% (A) ; from 5 to 10 min: 100% (A)–0% (B) to 40% (A)–60% (B) ; from 10 to 48 min: 40% (A)–60% 5(B) to 30% (A)–70% (B) ; from 48 to 50 min : 30% (A)–70% (B) to 0% (A)–100% (B) ; from 50 to 55 min: 100% (B) ; from 55 to 60 min: 100% (B) to 100% (A) ; from 60 to 70 min: 100% (A) to yield 7 pure compounds: **1** (5.33 mg, t_R 30.19 min), **2** (1.06 mg, t_R 31.7 min), **3** (20.03 mg, t_R 32.24 min), **4** (6.02 mg, t_R 32.37 min), **5** (1.39 mg, t_R 33.1), **6** (6.68 mg, t_R 33.31 min) and **7** (0.81 mg, t_R 34.05 min).

Eremoxylarin D (**1**): amorphous solid; $[\alpha]_D$ + 70.3 (*c* 0.2, MeOH); UV (MeOH) λ_{max} (log ε) 218 (3.34) nm; ECD (7.2×10^{-4} M, MeOH) λ_{max} (θ) 215 (+68.77) nm; ^1H and ^{13}C (500 MHz) NMR data, see Table 1; HR-ESIMS *m/z* 403.2124 $[M-H]^-$ (calcd for $C_{23}H_{32}O_6$, 403.2126).

Eremoxylarin E (**2**): amorphous solid; $[\alpha]_D$ + 20.0 (*c* 0.1, MeOH); UV (MeOH) λ_{max} (log ε) 215 (4.17), 265 (3.89) nm; ECD (1.17×10^{-4} M, MeOH) λ_{max} (θ) 211 (+30.29), 220 (+33.50), 226 (+31.68), 259 (−14.58) nm ; ^1H and ^{13}C (500 MHz) NMR data, see Table 1; HR-ESIMS *m/z* 427.2125 ($[M-H]^-$) (calcd for $C_{25}H_{32}O_6$, 427.2126).

Eremoxylarin F (**3**): amorphous solid; $[\alpha]_D$ + 26.3 (*c* 0.8, MeOH); UV (MeOH) λ_{max} (log ε) 226 (4.13) nm; ECD (1.61×10^{-4} M, MeOH) λ_{max} (θ) 213 (−27.20), 232 (+23.04), 256 (−6.18), 287

(−1.56), 327 (−4.66) nm; ^{1}H and ^{13}C (500 MHz) NMR data, see Table 1; HR-ESIMS *m/z* 429.2282 ([M-H]$^{-}$) (calcd for $C_{25}H_{34}O_6$, 427.2283).

Eremoxylarin G (**4**): amorphous solid; $[\alpha]_D$ + 20.0 (*c* 0.3, MeOH); UV (MeOH) λ_{max} (log ε) 216 (3.29) nm; ECD (5.9 × 10^{-4} M, MeOH) λ_{max} (θ) 212 (+27.63), 217 (+26.72), 226 (+15.99), 259 (−5.78) nm; ^{1}H and ^{13}C (500 MHz) NMR data, see Table 1; HR-ESIMS *m/z* 441.2282 ([M-H]$^{-}$ (calcd pour $C_{26}H_{33}O_6$, 441.2283).

Eremoxylarin H (**5**): amorphous solid; $[\alpha]_D$ + 14.0 (*c* 0.1, MeOH); UV (MeOH) λ_{max} (log ε) 213 (3.71) nm; ECD (2.3 × 10^{-4} M, MeOH) λ_{max} (θ) 212 (+16.74), 225 (+4.17), 230 (+4.91), 257 (−4.22) nm; ^{1}H and ^{13}C (500 MHz) NMR data, see Table 1; HR-ESIMS *m/z* 443.2352 ([M-H]$^{-}$) (calcd for $C_{26}H_{35}O_6$, 443.2439).

Eremoxylarin I (**6**): amorphous solid; $[\alpha]_D$ + 100.9 (*c* 0.2, MeOH); UV (MeOH) λ_{max} (log ε) 220 (3.90) nm; ECD (1.8 × 10^{-4} M, MeOH) λ_{max} (θ) 214 (+17.18), 219 (+15.52), 227 (−2.16), 233 (+8.50), 246 (−30.47), 323 (−6.66) nm; ^{1}H and ^{13}C (500 MHz) NMR data, see Table 1; HR-ESIMS *m/z* 443.2439 ([M-H]-) (calcd for $C_{26}H_{35}O_6$, 443.2439).

Eremoxylarin J (**7**): amorphous solid; $[\alpha]_D$ + 10.0 (*c* 0.1, MeOH); UV (MeOH) λ_{max} (log ε) 215 (4.29), 263 (4.37) nm; ECD (9.0 × 10^{-5} M, MeOH) λ_{max} (θ) 224 (+68.35), 262 (−37.55) nm; ^{1}H and ^{13}C (500 MHz) NMR data, see Table 1; HR-ESIMS *m/z* 455.2438 ([M-H]$^{-}$) (calcd for $C_{27}H_{35}O_6$, 455.2439).

Computational method. The coordinates of the lowest energy conformer of compounds **1**–**7** were optimized by TD-DFT of the type B3LYP/6-31G(d).[25–27] The vibrational

analysis in the harmonic approximation was performed at the same level of theory after convergence of the geometric optimization, and the local minimum was characterized by the absence of imaginary frequency. The excitation energies and corresponding rotational forces for the first 60 electronic transitions were then calculated by the TD-DFT method[28] at the B3LYP/6-31G* level. The ECD spectrum was calculated by Gaussian function summation[29] using SpecDis v1.64 software.[30] Bandpass values and any hypsochromic or bathochromic shifts (where applicable) are shown in the plots showing the superposition of the experimental and TD-DFT calculated ECD spectra for all compounds **1**-**7**.

Antibacterial assays. Antibacterial activity assays were performed using the broth dilution technique in 96-well microplates in triplicate. *S. aureus* sensitive and resistant (CIP 53.156 and DSM 13661), *S. epidermidis* (CIP 53.124), *E. coli* (CIP 54.8) and *P. aeruginosa* (CIP A22) were provided by the NuMeCan team (Nutrition, Métabolismes et Cancer), University of Rennes. These strains were grown at 37 °C using Luria Broth (LB) medium (2.5 g peptone, 2.5 g NaCl, 1.5 g yeast extract and 500 mL distilled water). The compounds were prepared in pure DMSO (D2650 Sigma Aldrich) at 5 mg/mL for tested compounds and 10 mg/mL for gentamicin (G1272 – 10 mL Sigma Aldrich) as positive control. According to the Clinical and Laboratory Standards Institute (CLSI) (National Committee for Clinical Laboratory Standards, 2004), the compounds were serially diluted 1:2 in LB in a sterile 96-well plate. Each well was then inoculated with 10^6 CFU/mL of each strain for 24 h at 37 °C. The solvents used to prepare the compounds were also tested on the bacteria as negative control. All the wells were then plated on LB agar and incubated for 24 h at 37 °C. Optical density measurements were made at 630 nm using an Allsheng AMR100 reader (Hangzhou Allsheng instruments Co., Ltd., China) before and after incubation to obtain growth inhibition values.

Subsequently, the MIC, defined as the minimal concentration able to inhibit the visible bacterial growth, was determined as the clear well having the lowest concentration.

Antiviral and Cytotoxic assays. The chemicals, Dulbecco's modified Eagle's medium (DMEM) with glutaMAX-I was purchased from Life Technologies. Foetal bovine sera (FBS) was obtained from Eurobio. Stocks of compounds were resuspended in DMSO (D2650 Sigma Aldrich) at 100 mM respectively. Human hepatoma cell line Huh-7 and the stable cell line expressing TMPRSS2 (Huh-7/TMPRSS2) were grown in DMEM with glutaMAX-I and 10% FBS in an incubator at 37 °C with 5% CO_2. The viral recombinant HCoV-229E-Luc were used (kind gift of Pr. V. Thiel). The cell toxicity assay was performed as following: 6×10^4 Huh-7 cells were seeded in 96-well plates and incubated for 16 h at 37 °C 5% CO_2 incubator. The cells were then treated with increasing concentrations of each compound for 24 h. An MTS [3-(4,5-dimethylthiazol-2-yl)-5-(3-carboxymethoxyphenyl)-2-(4-sulfophenyl)-2H-tetrazolium]-based viability assay (Cell Titer 96 Aqueous non-radioactive cell proliferation assay, Promega) was performed as recommended by the manufacturer. The absorbance of formazan at 490 nm was detected using a plate reader (ELX 808 Bio-Tek Instruments Inc). For antiviral assays, Huh-7 and Huh-7/TMPRSS2 cells were inoculated with HCoV-229E-Luc at a MOI of 0.5 in a final volume of 50 µL for 1 h at 37 °C in the presence of each compound at increasing concentrations. The virus was removed and replaced with culture medium containing the different compounds for 6 h at 37 °C. Cells were lysed in 20 µL of Renilla Lysis Buffer (Promega, Madison, USA) and luciferase activity was quantified in a Tristar LB 941 luminometer (Berthold Technologies, Bad Wildbad, Germany) using Renilla Luciferase Assay System (Promega) as recommended by the manufacturer. Each measure was performed in triplicate and each experiment was repeated 3 times.

ASSOCIATED CONTENT

Supporting Information

The Supporting Information is available free of charge at xxx. 1D and 2D NMR data for **1**−**7**.

AUTHOR INFORMATION

Corresponding Author

Sophie Tomasi – *Univ Rennes, CNRS, ISCR-UMR 6226, Rennes, France;* orcid.org/0000-0001-9827-527X; Phone: + 33 2 23 23 48 17; E-mail: sophie.tomasi@univ-rennes1.fr

Author Contributions

The manuscript was written through contributions of all authors. All authors have given approval to the final version of the manuscript.

Notes

The authors declare no competing financial interest

ACKNOWLEDGMENTS

Circular dichroism recordings were performed using the Spectroscopies-CDTP core facility (UMS Biosit, Université de Rennes - Campus de Villejean- 35043 RENNES Cedex, FRANCE) and HR-MS analysis using CRMPO core facility (ScanMatn Université de Rennes 1 – Campus de Beaulieu -35043 RENNES Cedex, FRANCE). NMR experiments were performed using the PRISM core facility (Biogenouest, Univ Rennes, Univ Angers, INRAE, CNRS, FRANCE). Leo Goehrs (Alionis) is gratefully acknowledged for the donation of the computing hardware.

References

(1) Ji, H.-F.; Li, X.-J.; Zhang, H.-Y. *EMBO Rep.* **2009**, *10*, 194–200.
(2) Wright, G. D. *Can. J. Microbiol.* **2014**, *60*, 147–154.
(3) Lam, K. S. *Trends Microbiol.* **2007**, *15*, 279–289.
(4) Hawksworth, D. L.; Grube, M. *New Phytol.* **2020**, *227*, 1281–1283.
(5) Yoon, V.; Nodwell, J. R. *J. Ind. Microbiol. Biotechnol.* **2014**, *41*, 415–424.
(6) Yim, G.; Huimi Wang, H.; Davies FRS, J. *Philos. Trans. R. Soc. B Biol. Sci.* **2007**, *362*, 1195–1200.
(7) Agrawal, S.; Deshmukh, S. K.; Reddy, M. S.; Prasad, R.; Goel, M. *South Afr. J. Bot.* **2020**, *134*, 163–186.
(8) Kellogg, J. J.; Raja, H. A. *Phytochem. Rev.* **2017**, *16*, 271–293.
(9) Miral, A.; Jargeat, P.; Mambu, L.; Rouaud, I.; Tranchimand, S.; Tomasi, S. *Environ. Microbiol. Rep.* **2022**.
(10) Büttner, E.; Liers, C.; Hofrichter, M.; Gebauer, A. M.; Kellner, H. *Microbiol. Resour. Announc.* **2019**.
(11) Renke, J.; Deters, A.; Kumar, N. S. *Planta Med.* **2012**, *78*, PI457.
(12) Hashemi, S. A.; Khodaparast, S. A.; Zare, R.; Elahinia, S. A. *Rostaniha* **2014**, *15*, 153–166.
(13) Jagadish, B. R.; Sridhar, K. R.; Dattaraj, H. R.; Chandramohana, N.; Mahadevakumar, S. In *Industrially Important Fungi for Sustainable Development: Volume 2: Bioprospecting for Biomolecules*; Abdel-Azeem, A. M., Yadav, A. N., Yadav, N., Sharma, M., Eds.; Fungal Biology; Springer International Publishing: Cham, 2021; pp 717–735.
(14) Kuhnert, E.; Navarro-Muñoz, J. C.; Becker, K.; Stadler, M.; Collemare, J.; Cox, R. J. *Stud. Mycol.* **2021**, *99*, 100118.
(15) Canli, K.; Akata, I.; Altuner, E. M. *Afr. J. Tradit. Complement. Altern. Med.* **2016**, *13*, 42–46.
(16) Özbey, B.; İşlek, C.; Baba, H.; Akata, I.; Sevindik, M. *Fresenius Environ. Bull.* **2021**, *30*, 5400–5404.
(17) McDonald, L. A.; Barbieri, L. R.; Bernan, V. S.; Janso, J.; Lassota, P.; Carter, G. T. *J. Nat. Prod.* **2004**, *67*, 1565–1567.
(18) Isaka, M.; Yangchum, A.; Supothina, S.; Chanthaket, R.; Srikitikulchai, P. *Phytochem. Lett.* **2014**, *8*, 59–64.
(19) Singh, S. B.; Zink, D.; Polishook, J.; Valentino, D.; Shafiee, A.; Silverman, K.; Felock, P.; Teran, A.; Vilella, D.; Hazuda, D. J.; Lingham, R. B. *Tetrahedron Lett.* **1999**, *40*, 8775–8779.
(20) Srisapoomi, T.; Ichiyanagi, T.; Nakajima, H.; Aimi, T.; Boonlue, S. *Chiang Mai J. Sci.* **2015**, *42*.
(21) Shiono, Y.; Murayama, T. *Z. Für Naturforschung B* **2005**, *60*, 885–890.
(22) Zhang, C.; Idelbayev, Y.; Roberts, N.; Tao, Y.; Nannapaneni, Y.; Duggan, B. M.; Min, J.; Lin, E. C.; Gerwick, E. C.; Cottrell, G. W.; Gerwick, W. H. *Sci. Rep.* **2017**, *7*, 14243.
(23) Leitgeb, A. J.; Feliciano, J. A.; Sanchez, H. A.; Allen, R. A.; Morrison, K. R.; Sommers, K. J.; Carden, R. G.; Wuest, W. M.; Minbiole, K. P. C. *ChemMedChem* **2020**, *15*, 667–670.
(24) Bertram, S.; Dijkman, R.; Habjan, M.; Heurich, A.; Gierer, S.; Glowacka, I.; Welsch, K.; Winkler, M.; Schneider, H.; Hofmann-Winkler, H.; Thiel, V.; Pöhlmann, S. *J. Virol.* **2013**, *87*, 6150–6160.
(25) Becke, A. D. *J. Chem. Phys.* **1993**, *98*, 5648–5652.
(26) Lee, C.; Yang, W.; Parr, R. G. *Phys. Rev. B* **1988**, *37*, 785–789.
(27) Shimkevich, A. *World J. Condens. Matter Phys.* **2014**, *4*, 243–249.

(28) Cai, Z.-L.; Reimers, J. R. *J. Chem. Phys.* **2000**, *112*, 527–530.
(29) Stephens, P. J.; Harada, N. *Chirality* **2010**, *22*, 229–233.
(30) Bruhn, T.; Schaumlöffel, A.; Hemberger, Y.; Bringmann, G. *Chirality* **2013**, *25*, 243–249.

TOC Graphic